HHS Public Access

Author manuscript

Pediatr Radiol. Author manuscript; available in PMC 2022 February 01.

Published in final edited form as:

Pediatr Radiol. 2022 February ; 52(2): 354–366. doi:10.1007/s00247-021-05098-5.

How to stop using gadolinium chelates for MRI: Clinical-translational experiences with ferumoxytol

Heike E. Daldrup-Link, MD, PhD[1,2,*], **Ashok J. Theruvath, MD**[1,*], **Ali Rashidi, MD**[1,*], **Michael Iv, MD**[1,*], **Robbie G. Majzner, MD, PhD**[2,*], **Sheri L. Spunt, MD, MBA**[2,*], **Stuart Goodman, MD, PhD**[3,*], **Michael Moseley, PhD**[1,*]

[1]Department of Radiology, Molecular Imaging Program at Stanford (MIPS), Stanford University

[2]Department of Pediatrics, Division of Hematology/Oncology, Stanford University

[3]Department of Orthopedic Surgery, Stanford University

Abstract

Gadolinium chelates have been used as standard contrast agents for clinical magnetic resonance imaging (MRI) for several decades. However, several investigators recently reported that rare earth metals such as gadolinium are deposited in the brain for months or years. This is particularly concerning for children, whose developing brain is more vulnerable to exogenous toxins compared to adults. Therefore, a search is under way for alternative MR imaging biomarkers. The FDA-approved iron supplement ferumoxytol can solve this unmet clinical need: Ferumoxytol consists of iron oxide nanoparticles that can be detected with MRI and provide significant T1- and T2-signal enhancement of vessels and soft tissues. Several investigators including our own research group started to use ferumoxytol “off label” as a new contrast agent for MRI. This article will review the existing literature on the biodistribution of ferumoxytol in children and compare the diagnostic accuracy of ferumoxytol- and gadolinium chelate enhanced MRI. Iron oxide nanoparticles represent a promising new class of contrast agents for pediatric MRI, which can be metabolized and are not deposited in the brain.

Keywords

Children; Contrast agent; Ferumoxytol Iron oxide nanoparticles; Magnetic Resonance Imaging

Introduction

Contrast-enhanced MRI is essential for the diagnosis of traumatic injuries [1], tissue ischemia [2, 3], infection/inflammation [4, 5] and cancer [6-8]. Intravascular contrast improves the delineation of vessels and blood flow patterns characteristic of various disease states [8-12]. However, classical small molecular gadolinium-chelates are associated with significant side effects: In patients with impaired renal function, gadolinium-chelates can

*Corresponding author: Heike E. Daldrup-Link, M.D., Ph.D., Department of Radiology and Molecular Imaging Program at Stanford, Lucile Packard Children’s Hospital, Stanford University, 725 Welch Rd, Stanford, CA 94305-5614, Ph: (650) 723-8996, Fax: (650) 725-8957, H.E.Daldrup-Link@stanford.edu.

exacerbate renal toxicity [13] or cause nephrogenic systemic sclerosis [14-16]. In addition, there is mounting concern about long-term Gadolinium deposition in the basal ganglia and dentate nucleus of the brain. [17-19] Among different formulations, linear gadolinium-chelates have been associated with a higher risk of nephogenic systemic sclerosis (NSF) [20] and a higher risk of brain deposition due to a higher dissociation of Gadolinium from the chelate [21]. Macrocyclic gadolinium-chelates are considered more stable, although there are also reports of NSF [20] and macrocyclic gadolinium-chelate deposition in the brain [18, 22]. While effects of gadolinium deposition on the neurocogntitive function in humans are currently unknown, negative effects have been described in animal models: In animals, gadolinium-chelates that crossed the blood brain barrier caused significant neurotoxicity, including behavioral changes, acute excitation, myoclonus, ataxia and seizures. [23, 24] Evidence from case reports suggests that gadolinium deposition also occurs in the brains of children, with a similar deposition pattern to that observed in adults and animal models [25, 26]. This is particularly concerning, since the developing brain is more vulnerable to exogenous toxins compared to adults [27, 28] and long-term consequences of gadolinium-depositions in the developing brain are unknown. Hence, there is an active search for gadolinium-free MRI protocols for pediatric patients.

Although clinical MRI applications since 1983 primarily focused on the use of Gadolinium-chelates as contrast agents, MR investigators had already identified iron oxides as alternate MR contrast agents with high r1 and r2 relaxivities [29]. The FDA approved iron supplement ferumoxytol (Feraheme) is perhaps the most widely clinically applied iron oxide compound to date, having been administered to more than one million adult patients for the treatment of anemia [30]. Ferumoxytol is composed of iron oxide nanoparticles with a 6.4-7.2 nm iron oxide core and a 28-32 nm carboxymethyldextran coat [31-33]. The large size of ferumoxytol nanoparticles leads to their prolonged circulation in the blood pool and resultant strong and long-lasting MR signal effects [30]. Since it can be detected with MRI, several investigators started to use ferumoxytol “off label” as a contrast agent in adult patients undergoing MRI scans [34-38]. Ferumoxytol nanoparticles are metabolized in the liver and are not associated with any direct or indirect renal toxicity, a potential benefit relative to clinical standard contrast agents [31, 33, 39-41]. Therefore, ferumoxytol can fill an important gap for imaging evaluations of patients with renal insufficiency. In addition, biodistribution studies in adult patients have shown that ferumoxytol does not cross the blood brain barrier in the normal brain [30]. Ferumoxytol is incorporated into the body’s iron metabolism and slowly metabolized by the reticuloendothelial system (RES) [30]. Therefore, it is relatively contra-indicated in patients with hemosiderosis or hemochromatosis. Since ferumoxytol does not cause any renal toxicity and does not cross the blood brain barrier of the normal brain, it is an attractive candidate to preplace gadolinium-chelates for pediatric MRI studies.

While several investigators including our own group started to use ferumoxytol nanoparticles for MR angiography [30] and MR imaging of vascular malformations [42], cardiovascular abnormalities [43] and tumors in children [44], head-to-head comparisons of gadolinium-chelate enhanced MRI and ferumoxytol-MRI scans are scarce. This article will summarize the current knowledge regarding ferumoxytol-enhanced MRI studies in pediatric patients.

Safety of iron oxide nanoparticles

The development and clinical translation of ferumoxytol builds on extensive preclinical [45-49] and clinical [30, 44, 50-53] investigations of iron oxide nanoparticles. Ferumoxytol nanoparticles are generally well tolerated [30]. Doses up to 400 mg Fe/kg were non-lethal in rodents [54]. Ferumoxytol doses for MR imaging (1-5 mg Fe/kg) are significantly lower compared to FDA-approved doses for anemia treatment (2 x 510 mg per patient) [30, 44, 55]. Rare anaphylactic reactions have been described in adults, but not yet in children [31, 39, 56]. Likewise, our initial experience with ferumoxytol administrations in 49 pediatric patients did not reveal any side effects [57]. It is important to administer iron slowly in both adults and children, as recommended by the FDA in order to avoid hypotensive reactions, which are sometimes mistaken for allergic reactions [55]. We did not find significant changes of blood pressure and heart rate in the immediate post-administration period nor significant alternations of serum biomarkers for liver or renal function in pediatric patients over a 28 day observation period [57].

As a first step to establishing ferumoxytol as an alternative contrast agent to gadolinium-chelates, it is important to investigate whether ferumoxytol (and iron oxide nanoparticles in general) can be deposited in the brain of children. Experimental studies did not find evidence of iron deposition in the brains of mice or pigs, who had received a single (or in one case two) intravenous injection(s) of ferumoxytol at a dose of 5 mg Fe/kg [58]. R2* relaxation rates (which are proportional to tissue iron concentrations) of different deep grey matter structures were not significantly different compared to control animals that had not received any ferumoxytol [58]. In addition, a retrospective case-control study of 17 children and young adults who had received intravenous ferumoxytol demonstrated no significant differences in R2* values of deep gray matter compared to 21 age and sex-matched controls [59]. In patients who had received multiple transfusions, iron deposition in the choroid plexus has been observed [55]. Thus, further investigations about ferumoxytol deposition in the brain should specifically focus on signs of iron deposition in the plexus.

The typical imaging protcol involves administration of Ferumoxytol/Feraheme at a dose of 5 mg/kg. The original Ferumoxytol formulation, as supplied via the hospital pharmacy, has a concentration of 30 mg Fe/ml. A teenager with an average body weight of 50-80 kg will receive a total dose of 250-400 mg Fe (5 mg Fe/kg) or 8.3 – 13.3 ml of the original formulation, which is diluted 1:4 in saline and administered over at least 15 minutes.

Since ferumoxytol is a “blood pool agent” (i.e. providing long lasting vascular enhancement), it is not crucial for the quality of the imaging scan to administer the contrast agent while the patient is in the scanner or to start a post-contrast scan immediately after contrast media administration. Thus, we typically infuse diluted ferumoxytol slowly into a peripheral vein while the patient is outside of the MR scanner and under direct supervision. We observe the patient for at least 30 minutes, acquire vital signs and ask him/her for any subjective adverse effects. We continue to observe the patient closely during the MR scan. Since the majority of adverse events occur within the first 30 minutes of infusion, we cover the most sensitive time interval with this approach. This approach has been overall well tolerated by our patients [60, 61].

After a single intravenous administration of ferumoxytol at a dose of 1-5 mg Fe per kilogram body weight, the nanoparticles are slowly metabolized in organs of the reticuloendothelial system (RES), i.e. liver, spleen and bone marrow. Related signal effects on T2-weighted MRI images slowly decrease over time. Baseline MRI signal intensities are usually found after about 6-8 weeks [55]. However, age-, gender-, race/ethnicity- and co-morbidity-related variations in ferumoxytol metabolism remain a wide open area of investigation. In a limited study of six volunteers, a wide variation in ferumoxytol metabolism was observed, ranging from three months to 11 months [62]. It would be also important to study if pre-existing transfusional iron overload might lead to greater deposition of ferumoxytol in other tissues and/or longer periods of clearance.

Ferumoxytol nanoparticles for disease detection and treatment monitoring

Ferumoxytol provides significant blood pool enhancement for at least 24 hours, which can be used for MR angiography [36, 63, 64], tissue perfusion studies [38] and long-lasting vascular enhancement on whole body MR and PET/MR imaging studies [44]. The excellent vascular enhancement with ferumoxytol has been used for optimized detection of arteriovenous malformations (Figure 1) [59, 65], estimations of cerebral blood volume [66], detection of venous thrombosis [67] and evaluations of complex cardiovascular abnormalities [30]. Since ferumoxytol has been approved for treatment of iron deficiency in patients with anemia and ranal failure, assessments of creatinine lab values are not needed prior to a ferumoxtol-MRI [31, 61].

Gadolinium chelates and iron oxide nanoparticle enhanced MRI studies have been compared with regards to their sensitivity and specificity for the detection and characterization of tumors in adult patients, such as brain tumors [63, 68], breast tumors [69] and focal liver lesions [7, 70-72]. However, systematic comparisons in pediatric patients are scarce. We recently conducted the first systematic comparative investigation of the diagnostic accuracy of ferumoxytol- and gadolinium-enhanced MRI for assessment of bone and soft tissue sarcomas in children [73]. We found an overall equivalent performance of ferumoxytol- and gadolinium-chelate-enhanced MRI scans, while there were also some inherent differences between the two techniques (Figure 2): The posituve (bright) enhancement of the tumors on T1-weighted images was significantly stronger after intravenous administration of gadolinium chelates. This caused decreased tumor-to-muscle contrast on T1-weighted ferumoxytol-enhanced MRI scans, which however, could be compensated by unimpaired tumor-to-muscle contrast on T2-weighted scans [73]. Importantly, ferumoxytol-enhanced MRI scans provided improved tumor-to-vessel contrast and markedly improved detection of tumor thrombi compared to gadolinium-MRI scans, suggesting that this tracer may be more helpful for evaluating tumors especially in the preoperative period.

In the intermediate postcontrast phase, at 1-2 hours after intrvenous infusion, ferumoxytol nanoparticles extravasate across reticuloendothelial system sinuses and are slowly phagocytosed by macrophages, which leads to a negative (dark) signal of RES organs (but not malignant tumors) on T2-weighted MRI images. Malignant tumors do not show significant negative enhancement on T2-weighted images at 1-2 hours after intravenous infusion. This differential effect improved the diagnosis of malignant liver lesions (Figure 3)

[73], lymph nodes [74] and bone marrow [75]. Multiple investigators have reported that iron oxide nanoparticle-enhanced MRI detected more liver metastases than gadolinium-chelate enhanced MRI [70, 72, 73, 76]. In addition, ferumoxytol nanoparticles were retained in focal nodular hyperplasia (FNH), which allowed for MRI characterization of these lesions [36, 55], similar to the imaging concept with gadolinium-DTPA-EOB (Eovist), although the underlying physiology is different (Kupfer cell phagocytosis of ferumoxytol nanoparticles versus hepatocyte uptake and impaired biliary excretion of Gadolinium-DTPA-EOB in FNH).

Iron oxide nanoparticles slowly extravasate across the discontinuous endothelium of microvessels in malignant tumors. This extravasation is a process that takes several hours. While it requires some waiting time for the patient between ferumoxytol administration and imaging, a 24 hour delayed imaging scan can provide useful clinical information: Barajas et al reported that ferumoxytol-enhanced MRI demonstrated enhancement of growing tumors but not pseudoprogression, while gadolinium-enhanced MRI showed enhancement of both pathologies [63, 77]. Similarly, Hamilton et al. [68] found strong ferumoxytol-enhancement of dural metastases and no ferumoxytol-enhancement of meningiomas, while gadolinium-MRI showed enhancement of both. The underlying reason for the observed differential nanoparticle enhancement is likely leaky microvessels in malignant tumors and absence of nanoparticle leak into benign conditions.

Finally, several hours after intravenous infusion, the iron oxide nanoparticles in the tumor interstitium are slowly phagocytosed by macrophages. Experimental [78] and clinical studies [79, 80] have shown, that a retention of ferumoxytol nanoparticles in the tumor tissue at 24-48 hours post intravenous injection correlates with the density of tumor associated macrophages on histology. This effect can be used to monitor tumor response to macrophage-activating cancer immunotherapies [81, 82]. In a recent study, **we** investigated 20 patients with lymphoma and bone sarcoma (n=10 each) with ferumoxytol-enhanced MRI, followed by tumor biopsy/resection and macrophage staining. We found that tumor MRI enhancement at 24 hours after intravenous injection of ferumoxytol correlated with the quantity of tumor associated macrophages in sarcomas and lymphomas on histopathology [79]. Tumor T2* relaxation times showed a significant, inverse correlation with the quantity of CD163 positive macrophages on histology specimen of sarcomas ($r = -0.56$; $P = 0.007$) and lymphomas. ($r = -0.76$; $P = 0.010$). This new imaging test could help to stratify patients with macrophage rich tumors to immune-modulating immunotherapies and help to monitor these immunotherapies in clinical practice. A study in adult patients demonstrated that ferumoxytol-MRI can be similarly used for imaging tumor associated macrophages in high grade gliomas of the brain [80].

Following chemotherapy, ferumoxytol-enhanced MRI provided improved detection of tumor necrosis compared to T2 weighted MRI scans or gadolinium-enhanced T1 weighted MRI scans [83]. Traditional MRI sequences visualize liquefactive necrosis based on lack of contrast enhancement on gadolinium-enhanced T1 weighted MRI scans and central hyper-intensity on T2 weighted images [84]. Ferumoxytol-enhanced MRI can detect earlier stages of necosis. Hypoxia leads to increased tumor microvascular permeability [85], which in turn can lead to extravasation of ferumoxytol nanoparticles (Figure 4). The

longitudinal relaxivity (T1-effect) of iron oxide nanoparticles is linearly related to the ability of the nanoparticles to interact with protons [86]. Therefore, ferumoxytol nanoparticles in tumor necrosis demonstrate marked T1-enhancement on 24 postcontrast scans, while intracellularly compartmentalized ferumoxytol nanoparticles in tumor associated macrophages demonstrate predominant T2-signal effects, with little or no T1 enhancement. Intracellular compartmentalization suppresses the T1-effect of iron oxide nanoparticles [87]. Therefore, differences in T1- and T2-relaxivities of iron oxide nanoparticles can be used to discriminate the location of the nanoparticles in different histopathological compartments [86]. An increased T1-enhancement of the tumor center after chemotherapy is indicative of early tumor necrosis and is noted before central liquefaction is observed [86].

Ferumoxytol nanoparticles cause vascular enhancement for several days and tissue enhancement for several weeks. This has led to concerns that iron oxide nanoparticles could interfere with gadolinium-enhanced MRI studies. In addition to an increasing number of patients who are receiving ferumoxytol “off label” as an MRI contrast agent, ferumoxytol has been administered to more tha one million patients for anemia treatment. Thus, it is very likely that radiologists to date will encounter patients who have been exposed to ferumoxytol. Studies in more than 1000 patients demonstrated that iron oxide nanoparticles do not interact with or interfere with the biodistribution, imaging characteristics or renal elimination of gadolinium chelates [7, 72, 76, 88]. Dual-contrast MR imaging has been obtained after injecting iron oxide nanoparticles and then gadolinium chelates [72, 76, 88, 89] or vice versa [7]. Nevertheless, it will be important to understand tissue MR enhancement patterns after administration of ferumoxytol in order to avoid diagnostic errors.

Ferumoxytol nanoparticles for *in vivo* tracking of therapeutic cells

Our team has worked for more than ten years on the development of novel imaging approaches for *in vivo* tracking of therapeutic cells [34, 35, 37, 49, 52, 61, 78, 90-99]. Iron oxide nanoparticles can be used to label therapeutic cells with high efficiency *ex vivo*. Thus far, nanoparticle-labeled neural stem cells,[100] mesenchymal stromal cells [101] dendritic cells [102] and pancreatic islet cells [103] have been tracked in patients with MRI. An exciting new application of *ex vivo* labeling approaches is directed towards labeling of tumor-targeted CAR T-cells. Labeling CAR-T cells with ferumoxytol enabled *in vivo* detection and quantification of the tumor accumulation of the labeled cells, an important prerequisite for successful treatment outcomes.

E*x vivo* labeling with nanoparticles requires manipulation of the therapeutic cells and is not compatible with harvesting and transplanting the cells in one surgery. To solve this problem, we developed a conceptually new approach of *in vivo* labeling of therapeutic stem cells before the cells are harvested from bone marrow [98]. We have shown that intravenous ferumoxytol administration leads to uptake of the nanoparticles by cells in the bone marrow. After being harvested from bone marrow and transplanted into arthritic joints, the iron-labeled stem cells can be tracked with clinical MRI [98]. We recently conducted a first-in-patient clinical trial to demonstrate “proof-of-concept” of the safety and efficacy of ferumoxytol labeling for autologous stem cell transplants following core decompression for the treatment of osteonecrosis [104]. We found that ferumoxytol-labeled cells could

be detected via T2-weighted MRI (Figure 6). The ability to track stem cells after their transplantation in osteonecrosis lesions offered a non-invasive means to dynamically monitor stem cell engraftment *in vivo*. This new approach could be also applied to understand and optimize these cell therapies with regards to administered cell numbers, optimized cell delivery and co-treatments.

Limitations of Ferumoxytol Nanoparticles

Considering the fact that ferumoxytol nanoparticles are phagocytosed by macrophages, we investigated a number of additional potential applications, which however did not work out as anticipated: We hypothesized that we would find a stronger accumulation of iron oxide nanoparticles in osteomyelitis compared to malignant bone tumors, because infection/inflammation would be expected to have a higher number of macrophages. It turned out that both osteomyelitides and malignant bone tumors demonstrated a wide spectrum of iron oxide nanoparticle uptake and retention.

Similarly, we investigated ferumoxytol retention in renal allografts that underwent an immune rejection. In children and teenagers with kidney transplants, immunologically mediated rejection is a major cause of allograft failure. In a large multicenter study of 1667 pediatric allografts, 49% of the graft failures were caused by rejection, including 26% acute and 23% chronic rejections [105]. Children with kidney transplants currently undergo at least three routine (protocol) biopsies during the first two years after the transplantation [106, 107]. These biopsies are invasive and nearly always require general anesthesia, causing anxiety and distress of the patients and their parents, as well as significant costs to the patient and health care system. Recently, iron oxide nanoparticles were used to diagnose macrophage infiltration in acute cardiac allograft rejection in rats [108], acute pancreatic allograft rejection in rats [109] and humans [110] and renal allograft rejection in rats [111] and humans [112]. In renal allografts that underwent rejection, CD68-positive macrophages co-localized with areas of tissue-damage and fibrosis, were found in more severe forms of rejection and represented an independent predictor of worse outcomes [113-115]. We hypothesized that allograft rejection would lead to increased retention of ferumoxytol nanoparticles and resultant T2*-shortening on MR images compared to a healthy allograft. Surprisingly, we found the opposite effect: Allografts with acute rejection showed prolonged (rather than shortened) T2* values on ferumoxytol-enhanced MR images. This can be explained by reduced perfusion and edema of rejected allografts compared to healthy non-rejected transplants with diminished ferumoxytol perfusion. This observation agrees with previously reported perfusion studies with other contrast agents [116-118]. The absence of significant macrophage retention is likely because allograft rejection in patients is noticed at an early stage and severe, advanced rejection with high macrophage load is rare in clinical practice [105].

In addition, we have conducted the first experimental human study to investigate macrophage-mediated inflammation as a possible biomarker of migraine. Using ferumoxytol-enhanced 3T magnetic resonance imaging (MRI), we investigated the presence of macrophages in cerebral artery walls and in brain parenchyma of patients with migraine without aura. We investigated both patients who received anti-migraine medication and

patients who did not [119]. To validate our use of ferumoxytol-MRI, we included a preclinical model where subcutaneous capsaicin injection in the trigeminal V1 area confirmed that ferumoxytol-MRI can detect macrophage-mediated inflammation. However, in patients, migraine attacks were not associated with increased ferumoxytol signal, suggesting that migraine without aura is not associated with macrophage-mediated inflammation [119].

Summary

In summary, superparamagnetic iron oxide nanoparticles such as ferumoxytol represent an alternative to gadolinium chelates as biodegradable MRI contrast agents with excellent T1- and T2-signal effects. More systematic comparisons between gadolinium chelate and ferumoxytol-enhanced MRI applications are needed to inform decisions about which contrast agent is most useful in different clinical scenarios. Ferumoxytol may be superior to gadolinium chelate in some diagnostic settings. While there are no reports of long term deposition of ferumoxytol in the human brain thus far, the overall faster renal elimination of gadolinium chelates may be an important benefit, especially for pediatric patients who have to undergo short-term follow up studies. Considering the cell-specific uptake of ferumoxytol nanoparticles, there are many additional applications for stem cell imaging, macrophage and immune cell tracking that can be explored in different physiological and pathological contexts.

Acknowledgments:

This study was supported by a grant from the Eunice Kennedy Shriver National Institute of Child Health and Human Development (NICHD, R01 HD081123A) and the National Institute of Arthritis and Musculoskeletal and Skin Diseases (R01AR054458).

References

1. Huguet M, Tobon-Gomez C, Bijnens BH et al. (2009) Cardiac injuries in blunt chest trauma. Journal of cardiovascular magnetic resonance: official journal of the Society for Cardiovascular Magnetic Resonance 11:35. [PubMed: 19761581]
2. Huisman TA, Sorensen AG (2004) Perfusion-weighted magnetic resonance imaging of the brain: techniques and application in children. Eur Radiol 14:59–72. [PubMed: 12827431]
3. Kim RJ, Wu E, Rafael A, et al. (2000) The use of contrast-enhanced magnetic resonance imaging to identify reversible myocardial dysfunction. N Engl J Med 343:1445–1453. [PubMed: 11078769]
4. Rosenbaum DG, Askin G, Beneck DM, et al. (2017) Differentiating perforated from non-perforated appendicitis on contrast-enhanced magnetic resonance imaging. Pediatr Radiol 47:1483–1490. [PubMed: 28578474]
5. Sugimoto H, Takeda A, Hyodoh K (2001) MR imaging for evaluation of early rheumatoid arthritis. Semin Musculoskelet Radiol 5:159–165. [PubMed: 11500160]
6. Wakabayashi H, Saito J, Taki J, et al. (2016) Triple-phase contrast-enhanced MRI for the prediction of preoperative chemotherapeutic effect in patients with osteosarcoma: comparison with (99m)Tc-MIBI scintigraphy. Skeletal radiology 45:87–95. [PubMed: 26385785]
7. Simon G, Link TM, Wortler K, et al. (2005) Detection of hepatocellular carcinoma: comparison of Gd-DTPA- and ferumoxides-enhanced MR imaging. Eur Radiol 15:895–903. [PubMed: 15800773]
8. Clauser P, Helbich TH, Kapetas P, et al. (2019) Breast lesion detection and characterization with contrast-enhanced magnetic resonance imaging: Prospective randomized intraindividual comparison of gadoterate meglumine (0.15 mmol/kg) and gadobenate dimeglumine (0.075 mmol/kg) at 3T. Journal of magnetic resonance imaging: JMRI 49(4): 1157–65. [PubMed: 30552829]

9. Lohrke J, Frenzel T, Endrikat J, et al. (2016) 25 Years of Contrast-Enhanced MRI: Developments, Current Challenges and Future Perspectives. Adv Ther 33:1–28. [PubMed: 26809251]
10. Mikati AG, Tan H, Shenkar R, et al. (2014) Dynamic permeability and quantitative susceptibility: related imaging biomarkers in cerebral cavernous malformations. Stroke; a journal of cerebral circulation 45:598–601.
11. Daldrup-Link HE, Simon GH, Brasch RC (2006) Imaging of tumor angiogenesis: current approaches and future prospects. Current pharmaceutical design 12:2661–2672. [PubMed: 16842165]
12. Zhou Z, Lu ZR (2012) Gadolinium-based contrast agents for magnetic resonance cancer imaging. Wiley interdisciplinary reviews Nanomedicine and nanobiotechnology.
13. Perazella MA (2009) Current status of gadolinium toxicity in patients with kidney disease. Clin J Am Soc Nephrol 4:461–469. [PubMed: 19201920]
14. Bennett CL, Qureshi ZP, Sartor AO, et al. (2012) Gadolinium-induced nephrogenic systemic fibrosis: the rise and fall of an iatrogenic disease. Clinical kidney journal 5:82–88. [PubMed: 22833806]
15. Perazella MA (2009) Advanced kidney disease, gadolinium and nephrogenic systemic fibrosis: the perfect storm. Curr Opin Nephrol Hypertens 18:519–525. [PubMed: 19623065]
16. Thomsen HS, Morcos SK, Almen T, et al. (2013) Nephrogenic systemic fibrosis and gadolinium-based contrast media: updated ESUR Contrast Medium Safety Committee guidelines. Eur Radiol 23:307–318. [PubMed: 22865271]
17. McDonald RJ, McDonald JS, Kallmes DF, et al. (2015) Intracranial Gadolinium Deposition after Contrast-enhanced MR Imaging. Radiology 275:772–782. [PubMed: 25742194]
18. Kanda T, Matsuda M, Oba H, et al. (2015) Gadolinium Deposition after Contrast-enhanced MR Imaging. Radiology 277:924–925. [PubMed: 26599932]
19. Guo BJ, Yang ZL, Zhang LJ (2018) Gadolinium Deposition in Brain: Current Scientific Evidence and Future Perspectives. Front Mol Neurosci 11:335. [PubMed: 30294259]
20. Endrikat J, Dohanish S, Schleyer N, et al. (2018) 10 Years of Nephrogenic Systemic Fibrosis: A Comprehensive Analysis of Nephrogenic Systemic Fibrosis Reports Received by a Pharmaceutical Company from 2006 to 2016. Invest Radiol 53:541–550. [PubMed: 29547493]
21. Sherry AD, Caravan P, Lenkinski RE (2009) Primer on gadolinium chemistry. Journal of magnetic resonance imaging : JMRI 30:1240–1248. [PubMed: 19938036]
22. Murata N, Gonzalez-Cuyar LF, Murata K, et al. (2016) Macrocyclic and Other Non-Group 1 Gadolinium Contrast Agents Deposit Low Levels of Gadolinium in Brain and Bone Tissue: Preliminary Results From 9 Patients With Normal Renal Function. Invest Radiol 51:447–453. [PubMed: 26863577]
23. Roman-Goldstein SM, Barnett PA, McCormick CI, et al. (1991) Effects of gadopentetate dimeglumine administration after osmotic blood-brain barrier disruption: toxicity and MR imaging findings. AJNR American journal of neuroradiology 12:885–890. [PubMed: 1950917]
24. Ray DE, Cavanagh JB, Nolan CC, et al. (1996) Neurotoxic effects of gadopentetate dimeglumine: behavioral disturbance and morphology after intracerebroventricular injection in rats. AJNR American journal of neuroradiology 17:365–373. [PubMed: 8938312]
25. Miller JH, Hu HH, Pokorney A, et al. (2015) MRI Brain Signal Intensity Changes of a Child During the Course of 35 Gadolinium Contrast Examinations. Pediatrics 136:e1637–1640. [PubMed: 26574593]
26. Roberts DR, Holden KR (2016) Progressive increase of T1 signal intensity in the dentate nucleus and globus pallidus on unenhanced T1-weighted MR images in the pediatric brain exposed to multiple doses of gadolinium contrast. Brain Dev 38:331–336. [PubMed: 26345358]
27. Costa LG, Aschner M, Vitalone A, et al. (2004) Developmental neuropathology of environmental agents. Annu Rev Pharmacol Toxicol 44:87–110. [PubMed: 14744240]
28. Lanphear BP (2015) The impact of toxins on the developing brain. Annu Rev Public Health 36:211–230. [PubMed: 25581143]
29. Weinmann HJ, Brasch RC, Press WR, et al. (1984) Characteristics of gadolinium-DTPA complex: a potential NMR contrast agent. AJR Am J Roentgenol 142:619–624. [PubMed: 6607655]

30. Toth GB, Varallyay CG, Horvath A, et al. (2017) Current and potential imaging applications of ferumoxytol for magnetic resonance imaging. Kidney Int 92:47–66. [PubMed: 28434822]
31. Lu M, Cohen MH, Rieves D, et al. (2010) FDA report: Ferumoxytol for intravenous iron therapy in adult patients with chronic kidney disease. American journal of hematology 85:315–319. [PubMed: 20201089]
32. Balakrishnan VS, Rao M, Kausz AT, et al. (2009) Physicochemical properties of ferumoxytol, a new intravenous iron preparation. Eur J Clin Invest 39:489–496. [PubMed: 19397688]
33. Schwenk MH (2010) Ferumoxytol: a new intravenous iron preparation for the treatment of iron deficiency anemia in patients with chronic kidney disease. Pharmacotherapy 30:70–79. [PubMed: 20030475]
34. Khurana A, Nejadnik H, Chapelin F, et al. (2013) Ferumoxytol: a new, clinically applicable label for stem-cell tracking in arthritic joints with MRI. Nanomedicine (Lond) 8:1969–1983. [PubMed: 23534832]
35. Khurana A, Nejadnik H, Gawande R, et al. (2012) Intravenous ferumoxytol allows noninvasive MR imaging monitoring of macrophage migration into stem cell transplants. Radiology 264:803–811. [PubMed: 22820731]
36. Neuwelt EA, Varallyay CG, Manninger S, et al. (2007) The potential of ferumoxytol nanoparticle magnetic resonance imaging, perfusion, and angiography in central nervous system malignancy: a pilot study. Neurosurgery 60:601–611; discussion 611-602. [PubMed: 17415196]
37. Simon GH, von Vopelius-Feldt J, Fu Y, et al. (2006) Ultrasmall supraparamagnetic iron oxide-enhanced magnetic resonance imaging of antigen-induced arthritis: a comparative study between SHU 555 C, ferumoxtran-10, and ferumoxytol. Invest Radiol 41:45–51. [PubMed: 16355039]
38. Stabi KL, Bendz LM (2011) Ferumoxytol use as an intravenous contrast agent for magnetic resonance angiography. The Annals of pharmacotherapy 45:1571–1575. [PubMed: 22045905]
39. Singh A, Patel T, Hertel J, et al. (2008) Safety of ferumoxytol in patients with anemia and CKD. Am J Kidney Dis 52:907–915. [PubMed: 18824288]
40. Spinowitz BS, Kausz AT, Baptista J, et al. (2008) Ferumoxytol for treating iron deficiency anemia in CKD. Journal of the American Society of Nephrology : JASN 19:1599–1605. [PubMed: 18525001]
41. Spinowitz BS, Schwenk MH, Jacobs PM, et al. (2005) The safety and efficacy of ferumoxytol therapy in anemic chronic kidney disease patients. Kidney Int 68:1801–1807. [PubMed: 16164657]
42. Iv M, Choudhri O, Dodd RL, et al. (2018) High-resolution 3D volumetric contrast-enhanced MR angiography with a blood pool agent (ferumoxytol) for diagnostic evaluation of pediatric brain arteriovenous malformations. Journal of neurosurgery Pediatrics 22:251–260. [PubMed: 29882734]
43. Lai LM, Cheng JY, Alley MT, et al. (2017) Feasibility of ferumoxytol-enhanced neonatal and young infant cardiac MRI without general anesthesia. Journal of magnetic resonance imaging : JMRI 45:1407–1418. [PubMed: 27678106]
44. Muehe AM, Theruvath AJ, Lai L, et al. (2018) How to Provide Gadolinium-Free PET/MR Cancer Staging of Children and Young Adults in Less than 1 h: the Stanford Approach. Molecular imaging and biology : MIB 20:324–335. [PubMed: 28721605]
45. Mohanty S, Chen Z, Li K, et al. (2017) A Novel Theranostic Strategy for MMP-14-Expressing Glioblastomas Impacts Survival. Molecular cancer therapeutics 16:1909–1921. [PubMed: 28659432]
46. Zanganeh S, Hutter G, Spitler R, et al. (2016) Iron oxide nanoparticles inhibit tumour growth by inducing pro-inflammatory macrophage polarization in tumour tissues. Nature nanotechnology 11:986–994.
47. Nejadnik H, Lenkov O, Gassert F, et al. (2016) Macrophage phagocytosis alters the MRI signal of ferumoxytol-labeled mesenchymal stromal cells in cartilage defects. Scientific reports 6:25897. [PubMed: 27174199]
48. Iv M, Telischak N, Feng D, et al. (2015) Clinical applications of iron oxide nanoparticles for magnetic resonance imaging of brain tumors. Nanomedicine (Lond) 10:993–1018. [PubMed: 25867862]

49. Shi Q, Pisani LJ, Lee YK, et al. (2013) Evaluation of the novel USPIO GEH121333 for MR imaging of cancer immune responses. Contrast Media Mol Imaging 8:281–288. [PubMed: 23606432]
50. Daldrup-Link HE, Mohanty A, Cuenod C, et al. (2009) New perspectives on bone marrow contrast agents and molecular imaging. Semin Musculoskelet Radiol 13:145–156. [PubMed: 19455477]
51. Daldrup-Link HE, Henning T, Link TM (2007) MR imaging of therapy-induced changes of bone marrow. Eur Radiol 17:743–761. [PubMed: 17021706]
52. Metz S, Lohr S, Settles M, et al. (2006) Ferumoxtran-10-enhanced MR imaging of the bone marrow before and after conditioning therapy in patients with non-Hodgkin lymphomas. Eur Radiol 16:598–607. [PubMed: 16284770]
53. Daldrup-Link HE, Rydland J, Helbich TH, et al. (2003) Quantification of breast tumor microvascular permeability with feruglose-enhanced MR imaging: initial phase II multicenter trial. Radiology 229:885–892. [PubMed: 14576446]
54. Patsialou A, Wyckoff J, Wang Y, et al. (2009) Invasion of human breast cancer cells in vivo requires both paracrine and autocrine loops involving the colony-stimulating factor-1 receptor. Cancer Res 69:9498–9506. [PubMed: 19934330]
55. Daldrup-Link H (2017) 10 Things you might not know about Iron Oxide Nanoparticles. Radiology 284:616–629. [PubMed: 28825888]
56. Hassan N, Cahill J, Rajasekaran S, et al. (2011) Ferumoxytol infusion in pediatric patients with gastrointestinal disorders: first case series. The Annals of pharmacotherapy 45:e63. [PubMed: 22116997]
57. Muehe AM, Feng D, von Eyben R, et al. (2016) Safety Report of Ferumoxytol for Magnetic Resonance Imaging in Children and Young Adults. Invest Radiol 51:221–227. [PubMed: 26656202]
58. Theruvath AJ, Aghighi M, Iv M, et al. (2020) Brain iron deposition after Ferumoxytol-enhanced MRI: A study of Porcine Brains. Nanotheranostics 4:195–200. [PubMed: 32637297]
59. Iv M, Ng NN, Nair S, et al. (2020) Brain Iron Assessment after Ferumoxytol-enhanced MRI in Children and Young Adults with Arteriovenous Malformations: A Case-Control Study. Radiology 297:438–446. [PubMed: 32930651]
60. Muehe AM, Feng D, von Eyben R, et al. (2015) Safety Report of Ferumoxytol for Magnetic Resonance Imaging in Children and Young Adults. Investigative radiology.
61. Klenk C, Gawande R, Uslu L, et al. (2014) Ionising radiation-free whole-body MRI versus (18)F-fluorodeoxyglucose PET/CT scans for children and young adults with cancer: a prospective, non-randomised, single-centre study. The lancet oncology 15:275–285. [PubMed: 24559803]
62. Storey P, Lim RP, Chandarana H, Rosenkrantz AB, et al. (2012) MRI assessment of hepatic iron clearance rates after USPIO administration in healthy adults. Invest Radiol 47:717–724. [PubMed: 23070094]
63. Barajas RF Jr., Hamilton BE, Schwartz D, et al. (2018) Combined Iron Oxide Nanoparticle Ferumoxytol and Gadolinium Contrast Enhanced MRI Defines Glioblastoma Pseudo-progression. Neuro Oncol 21(4): 517–26.
64. Li W, Tutton S, Vu AT, Pierchala L, et al. (2005) First-pass contrast-enhanced magnetic resonance angiography in humans using ferumoxytol, a novel ultrasmall superparamagnetic iron oxide (USPIO)-based blood pool agent. Journal of magnetic resonance imaging : JMRI 21:46–52. [PubMed: 15611942]
65. Dosa E, Tuladhar S, Muldoon LL, et al. (2011) MRI using ferumoxytol improves the visualization of central nervous system vascular malformations. Stroke; a journal of cerebral circulation 42:1581–1588.
66. Pohlmann A, Karczewski P, Ku MC, et al. (2014) Cerebral blood volume estimation by ferumoxytol-enhanced steady-state MRI at 9.4 T reveals microvascular impact of alpha1 -adrenergic receptor antibodies. NMR in biomedicine 27:1085–1093. [PubMed: 25060359]
67. Li W, Salanitri J, Tutton S, et al. (2007) Lower extremity deep venous thrombosis: evaluation with ferumoxytol-enhanced MR imaging and dual-contrast mechanism--preliminary experience. Radiology 242:873–881. [PubMed: 17325072]

68. Hamilton BE, Woltjer RL, Prola-Netto J, et al. (2016) Ferumoxytol-enhanced MRI differentiation of meningioma from dural metastases: a pilot study with immunohistochemical observations. Journal of neuro-oncology 129:301–309. [PubMed: 27393348]
69. Daldrup-Link HE, Kaiser A, Helbich T, et al. (2003) Macromolecular contrast medium (feruglose) versus small molecular contrast medium (gadopentetate) enhanced magnetic resonance imaging: differentiation of benign and malignant breast lesions. Academic radiology 10:1237–1246. [PubMed: 14626298]
70. Vogl TJ, Hammerstingl R, Schwarz W, et al. (1996) Magnetic resonance imaging of focal liver lesions. Comparison of the superparamagnetic iron oxide resovist versus gadolinium-DTPA in the same patient. Invest Radiol 31:696–708. [PubMed: 8915751]
71. Lutz AM, Willmann JK, Goepfert K, et al. (2005) Hepatocellular carcinoma in cirrhosis: enhancement patterns at dynamic gadolinium- and superparamagnetic iron oxide-enhanced T1-weighted MR imaging. Radiology 237:520–528. [PubMed: 16192317]
72. Heilmaier C, Lutz AM, Bolog N, et al. (2009) Focal liver lesions: detection and characterization at double-contrast liver MR Imaging with ferucarbotran and gadobutrol versus single-contrast liver MR imaging. Radiology 253:724–733. [PubMed: 19789232]
73. Siedek F, Muehe AM, Theruvath AJ, et al. (2020) Comparison of ferumoxytol and Gd-chelate-enhanced MRI for assessment of bone and soft tissue sarcomas in children and young adults. Eur Radiol 30:1790–1803. [PubMed: 31844962]
74. Muehe AM, Siedek F, Theruvath AJ, et al. (2020) Differentiation of benign and malignant lymph nodes in pediatric patients on ferumoxytol-enhanced PET/MRI. Theranostics 10:3612–3621. [PubMed: 32206111]
75. Daldrup-Link HE, Rummeny EJ, Ihssen B, et al. (2002) Iron-oxide-enhanced MR imaging of bone marrow in patients with non-Hodgkin's lymphoma: differentiation between tumor infiltration and hypercellular bone marrow. Eur Radiol 12:1557–1566. [PubMed: 12042968]
76. Ward J, Guthrie JA, Scott DJ, et al. (2000) Hepatocellular carcinoma in the cirrhotic liver: double-contrast MR imaging for diagnosis. Radiology 216:154–162. [PubMed: 10887242]
77. Gahramanov S, Raslan AM, Muldoon LL, et al. (2010) Potential for Differentiation of Pseudoprogression from True Tumor Progression with Dynamic Susceptibility-weighted Contrast-enhanced Magnetic Resonance Imaging using Ferumoxytol vs. Gadoteridol: A Pilot Study. International journal of radiation oncology, biology, physics.
78. Daldrup-Link HE, Golovko D, Ruffel B, et al. (2011) MR Imaging of Tumor Associated Macrophages with Clinically-Applicable Iron Oxide Nanoparticles. Clin Cancer Res 17:5695–5704. [PubMed: 21791632]
79. Aghighi M, Theruvath AJ, Pareek A, et al. (2018) Magnetic Resonance Imaging of Tumor-Associated Macrophages: Clinical Translation. Clin Cancer Res 24:4110–4118. [PubMed: 29764855]
80. Iv M, Samghabadi P, Holdsworth S, et al. (2019) Quantification of Macrophages in High-Grade Gliomas by Using Ferumoxytol-enhanced MRI: A Pilot Study. Radiology 290:198–206. [PubMed: 30398435]
81. Mohanty S, Aghighi M, Yerneni K, et al. (2019) Improving the efficacy of osteosarcoma therapy: combining drugs that turn cancer cell 'don't eat me' signals off and 'eat me' signals on. Mol Oncol 13:2049–2061. [PubMed: 31376208]
82. Mohanty S, Yerneni K, Graef CM, et al. (2018) Imaging therapy response of osteosarcoma to anti-CD47 therapy. Cell Death & Disease 10:36–49.
83. Aghighi M, Golovko D, Ansari C, et al. (2015) Imaging Tumor Necrosis with Ferumoxytol. PLoS One 10:e0142665. [PubMed: 26569397]
84. Lim HS, Jeong YY, Kang HK, et al. (2006) Imaging features of hepatocellular carcinoma after transcatheter arterial chemoembolization and radiofrequency ablation. American Journal of Roentgenology 187:W341–W349. [PubMed: 16985104]
85. Fukumura D, Duda DG, Munn LL, et al. (2010) Tumor Microvasculature and Microenvironment: Novel Insights Through Intravital Imaging in Pre-Clinical Models. Microcirculation 17:206–225. [PubMed: 20374484]

86. Simon GH, Bauer J, Saborovski O, et al. (2006) T1 and T2 relaxivity of intracellular and extracellular USPIO at 1.5 T and 3T clinical MR scanning. European radiology 16:738–745. [PubMed: 16308692]
87. Turetschek K, Huber S, Floyd E, et al. (2001) MR Imaging Characterization of Microvessels in Experimental Breast Tumors by Using a Particulate Contrast Agent with Histopathologic Correlation 1. Radiology 218:562–569. [PubMed: 11161179]
88. Hanna RF, Kased N, Kwan SW, et al. (2008) Double-contrast MRI for accurate staging of hepatocellular carcinoma in patients with cirrhosis. AJR Am J Roentgenol 190:47–57. [PubMed: 18094293]
89. Guiu B, Loffroy R, Ben Salem D, et al. (2008) Combined SPIO-gadolinium magnetic resonance imaging in cirrhotic patients: negative predictive value and role in screening for hepatocellular carcinoma. Abdom Imaging 33:520–528. [PubMed: 17912584]
90. Daldrup-Link HE, Rudelius M, Piontek G, et al. (2005) Migration of iron oxide-labeled human hematopoietic progenitor cells in a mouse model: in vivo monitoring with 1.5-T MR imaging equipment. Radiology 234:197–205. [PubMed: 15618382]
91. Simon GH, Bauer J, Saborovski O, et al. (2006) T1 and T2 relaxivity of intracellular and extracellular USPIO at 1.5T and 3T clinical MR scanning. Eur Radiol 16:738–745. [PubMed: 16308692]
92. Simon GH, von Vopelius-Feldt J, Wendland MF, et al. (2006) MRI of arthritis: comparison of ultrasmall superparamagnetic iron oxide vs. Gd-DTPA. Journal of magnetic resonance imaging : JMRI 23:720–727. [PubMed: 16557494]
93. Henning TD, Sutton EJ, Kim A, et al. (2009) The influence of ferucarbotran on the chondrogenesis of human mesenchymal stem cells. Contrast Media Mol Imaging 4:165–173. [PubMed: 19670250]
94. Henning TD, Wendland MF, Golovko D, et al. (2009) Relaxation effects of ferucarbotran-labeled mesenchymal stem cells at 1.5T and 3T: discrimination of viable from lysed cells. Magnetic Resonance in Medicine 62:325–332. [PubMed: 19353670]
95. Nedopil A, Klenk C, Kim C, et al. (2010) MR signal characteristics of viable and apoptotic human mesenchymal stem cells in matrix-associated stem cell implants for treatment of osteoarthritis. Invest Radiol 45:634–640. [PubMed: 20808236]
96. Meier R, Golovko D, Tavri S, et al. (2011) Depicting adoptive immunotherapy for prostate cancer in an animal model with magnetic resonance imaging. Magnetic resonance in medicine : official journal of the Society of Magnetic Resonance in Medicine / Society of Magnetic Resonance in Medicine 65:756–763.
97. Henning TD, Gawande R, Khurana A, et al. (2012) Magnetic resonance imaging of ferumoxide-labeled mesenchymal stem cells in cartilage defects: in vitro and in vivo investigations. Molecular imaging 11:197–209. [PubMed: 22554484]
98. Khurana A, Chapelin F, Beck G, et al. (2013) Iron administration before stem cell harvest enables MR imaging tracking after transplantation. Radiology 269:186–197. [PubMed: 23850832]
99. Ansari C, Tikhomirov GA, Hong SH, et al. (2014) Cancer therapy: development of novel tumor-targeted theranostic nanoparticles activated by membrane-type matrix metalloproteinases for combined cancer magnetic resonance imaging and therapy (small 3/2014). Small 10:417.
100. Zhu J, Zhou L, XingWu F (2006) Tracking neural stem cells in patients with brain trauma. N Engl J Med 355:2376–2378. [PubMed: 17135597]
101. Callera F, de Melo CM (2007) Magnetic resonance tracking of magnetically labeled autologous bone marrow CD34+ cells transplanted into the spinal cord via lumbar puncture technique in patients with chronic spinal cord injury: CD34+ cells' migration into the injured site. Stem cells and development 16:461–466. [PubMed: 17610376]
102. de Vries IJ, Lesterhuis WJ, Barentsz JO, et al. (2005) Magnetic resonance tracking of dendritic cells in melanoma patients for monitoring of cellular therapy. Nat Biotechnol 23:1407–1413. [PubMed: 16258544]
103. Toso C, Vallee JP, Morel P, et al. (2008) Clinical magnetic resonance imaging of pancreatic islet grafts after iron nanoparticle labeling. American journal of transplantation : official journal of the American Society of Transplantation and the American Society of Transplant Surgeons 8:701–706.

104. Theruvath AJ, Nejadnik H, Muehe AM, et al. (2018) Tracking Cell Transplants in Femoral Osteonecrosis with Magnetic Resonance Imaging: A Proof-of-Concept Study in Patients. Clin Cancer Res 24:6223–6229. [PubMed: 30224340]
105. McEnery PT, Stablein DM, Arbus G, et al. (1992) Renal transplantation in children. A report of the North American Pediatric Renal Transplant Cooperative Study. N Engl J Med 326:1727–1732. [PubMed: 1594014]
106. Birk PE (2012) Surveillance biopsies in children post-kidney transplant. Pediatr Nephrol 27:753–760. [PubMed: 21792611]
107. Aghighi M, Pisani L, Theruvath AJ, et al. (2017) Ferumoxytol Is Not Retained in Kidney Allografts in Patients Undergoing Acute Rejection. Molecular imaging and biology : MIB : the official publication of the Academy of Molecular Imaging.
108. Wu YL, Ye Q, Eytan DF, et al. (2013) Magnetic resonance imaging investigation of macrophages in acute cardiac allograft rejection after heart transplantation. Circulation: Cardiovascular Imaging 6:965–973. [PubMed: 24097421]
109. Kriz J, Jirák D, Girman P, et al. (2005) Magnetic resonance imaging of pancreatic islets in tolerance and rejection. Transplantation 80:1596–1603. [PubMed: 16371931]
110. Evgenov NV, Medarova Z, Pratt J, et al. (2006) In vivo imaging of immune rejection in transplanted pancreatic islets. Diabetes 55:2419–2428. [PubMed: 16936189]
111. Chae EY, Song EJ, Sohn JY, et al. (2010) Allogeneic Renal Graft Rejection in a Rat Model: In Vivo MR Imaging of the Homing Trait of Macrophages 1. Radiology 256:847–854. [PubMed: 20720071]
112. Hauger O, Grenier N, Deminère C, et al. (2007) USPIO-enhanced MR imaging of macrophage infiltration in native and transplanted kidneys: initial results in humans. European radiology 17:2898–2907. [PubMed: 17929025]
113. Ricardo SD, van Goor H, Eddy AA (2008) Macrophage diversity in renal injury and repair. J Clin Invest 118:3522–3530. [PubMed: 18982158]
114. Magil AB (2009) Monocytes/macrophages in renal allograft rejection. Transplant Rev (Orlando) 23:199–208. [PubMed: 19640696]
115. Tinckam KJ, Djurdjev O, Magil AB (2005) Glomerular monocytes predict worse outcomes after acute renal allograft rejection independent of C4d status. Kidney Int 68:1866–1874. [PubMed: 16164665]
116. Thoeny HC, Zumstein D, Simon-Zoula S, et al. (2006) Functional evaluation of transplanted kidneys with diffusion-weighted and BOLD MR imaging: initial experience 1. Radiology 241:812–821. [PubMed: 17114628]
117. Sadowski EA, Djamali A, Wentland AL, et al. (2010) Blood oxygen level-dependent and perfusion magnetic resonance imaging: detecting differences in oxygen bioavailability and blood flow in transplanted kidneys. Magnetic resonance imaging 28:56–64. [PubMed: 19577402]
118. Wentland AL, Sadowski EA, Djamali A, et al. (2009) Quantitative MR measures of intrarenal perfusion in the assessment of transplanted kidneys: initial experience. Academic radiology 16:1077–1085. [PubMed: 19539502]
119. Khan S, Amin FM, Fliedner FP, et al. (2019) Investigating macrophage-mediated inflammation in migraine using ultrasmall superparamagnetic iron oxide-enhanced 3T magnetic resonance imaging. Cephalalgia 39:1407–1420. [PubMed: 31104505]

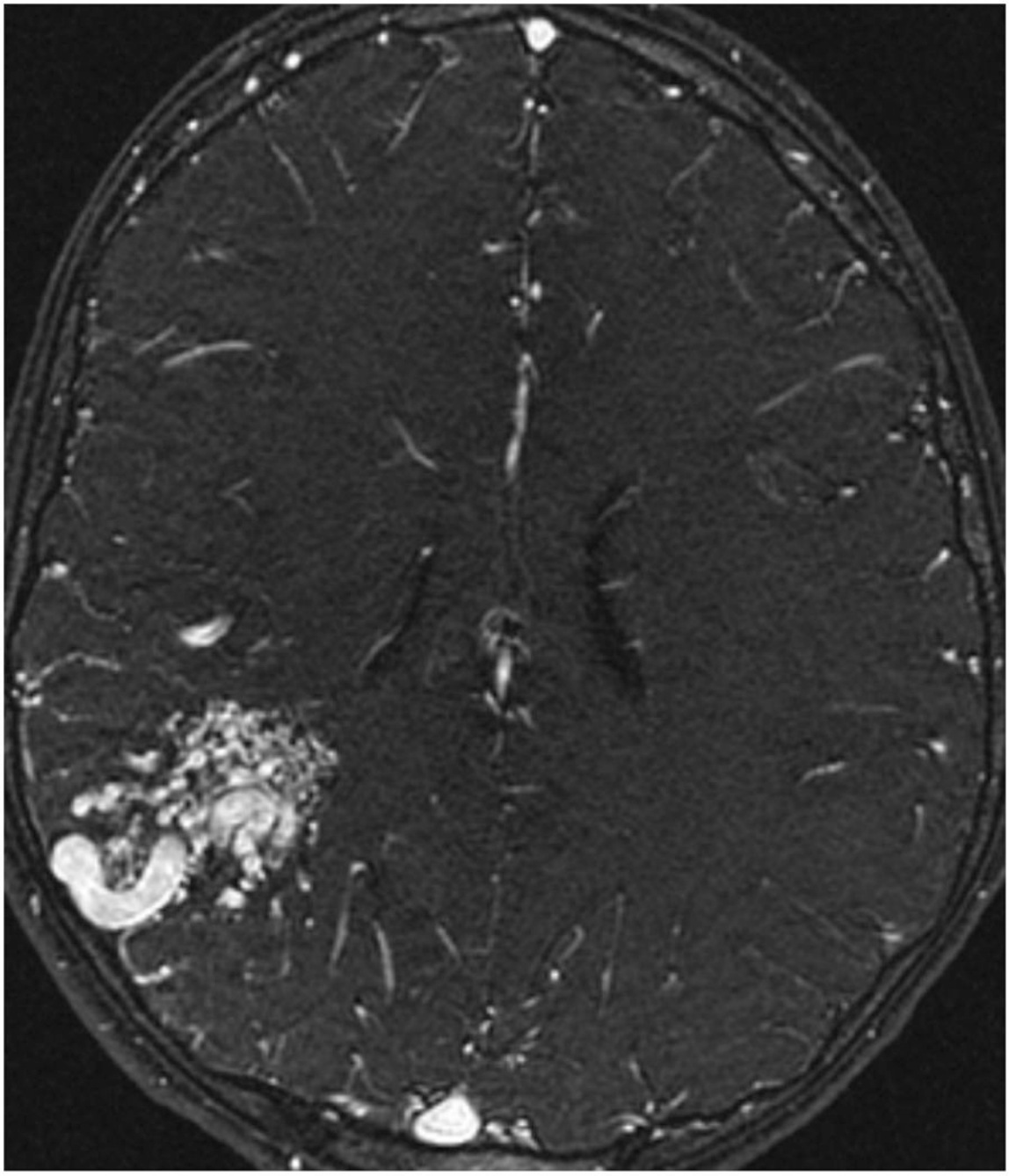

Figure 1: Ferumoxytol-MRI provides excellent vessel enhancement for MR angiographies.
Axial T1-weighted spoiled gradient recalled echo SPGR image at 10-15 minutes after intravenous infusion of ferumoxytol demonstrated a right parietal arteriovenous malformation in a 9-year-old boy. Note that for vascular imaging applications, a dose of 1-3 mg Fe/kg is usually sufficient. This patient received a dose of 3 mg Fe/kg.

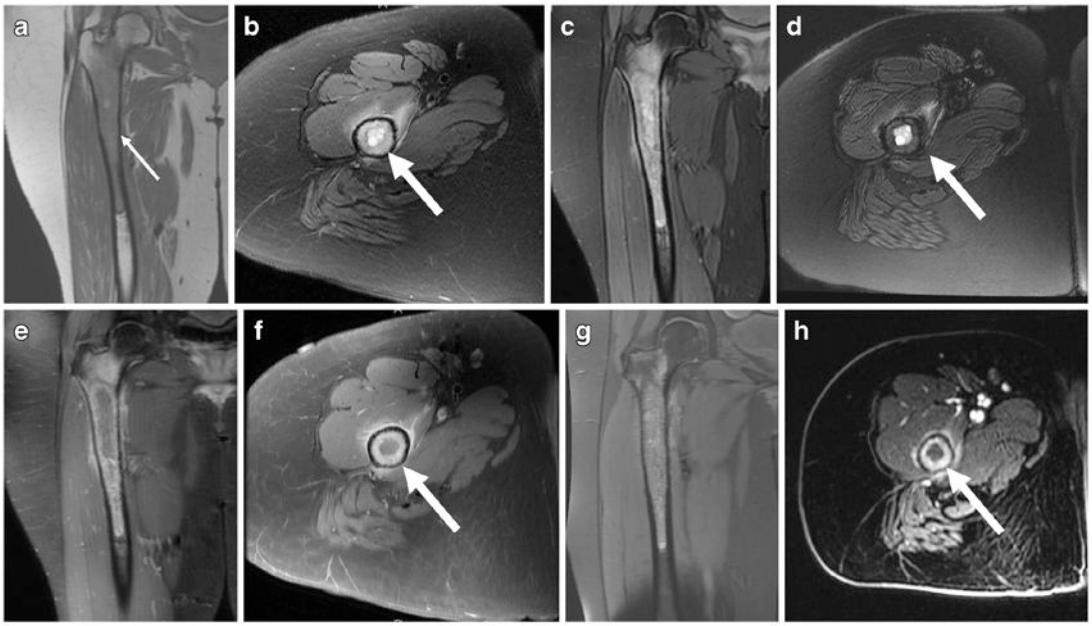

Figure 2: Comparison of tumor enhancement after intravenous administration of Gadolinium-chelate or ferumoxytol:

An osteosarcoma of the right proximal femur in 23 year old female demonstrates (a) hypointense signal on plain T1-weighted fast spin echo (FSE) image (arrow) as well as (b) hyperintense signal with regards to muscle as an internal standard on axial fat saturated T2-weighted FSE image and (c) coronal short inversion time inversion recovery (STIR) image. (d) Following intravenous administration of ferumoxytol (dose 5 mg Fe/kg), the peripheral tumor tissue demonstrates hypointense (dark) enhancement on T2-weighted FSE image, with sparing of a central area of necrosis (arrow). (e) A coronal T1-weighted scan and (f) an axial T1-weighted scan after intravenous injection of Gadolinium-chelate demonstrate corresponding peripheral enhancement of the tumor tissue (arrow), sparing of a central area of necrosis. (g) A coronal T1-weighted FSE image demonstrates hyperintense (positive) tumor enhancement, which is less intense compared to the Gadolinium-enhanced scan (e, f). (h) A delayed axial T1-weighted LAVA image about 10 minutes later demonstrates increasing tumor T1-enhancement over time (arrow), indicative of the accumulation of the nanoparticles in the tumor.

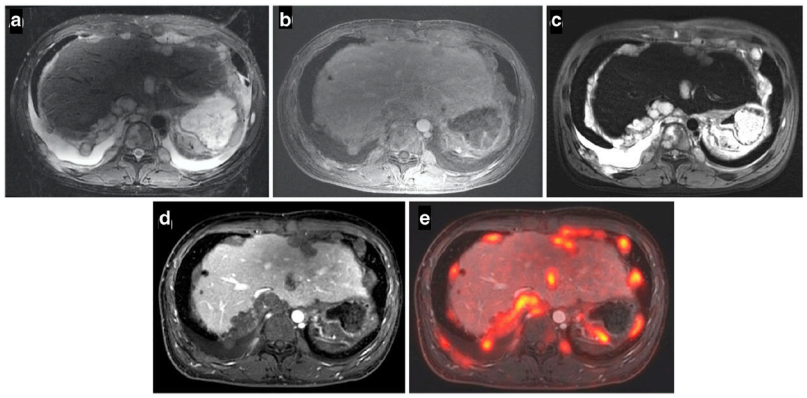

Figure 3: Comparison of tumor enhancement after intravenous administration of Gadolinium-chelate or ferumoxytol in a 25-year-old male with desmoplastic small round cell tumour:
(a) Axial T2-weighted MR image demonstrates intermediate T2-signal of the liver and multiple T2-hyperlintense focal tumor lesions along the liver capsule and the peritoneal lining. (b) A Gadolinium-chelate enhanced axial LAVA scan demonstrates moderate contrast enhancement of both liver and focal tumor lesions. (c) Ferumoxytol-enhanced axial T2-weighted fast spin echo (FSE) image shows negative (dark) enhancement of the liver and increased tumor-to-liver contrast. (d) Axial ferumoxytol-enhanced T1-weighted LAVA image shows less enhancement of the tumor compared to the liver, thereby increasing the tumor-to-liver contrast. (e) Simultaneously acquired axial ^{18}F-labeled fluorodeoxyglucose positron emission tomography (^{18}F-FDG PET) images was superimposed on T1-weighted axial ferumoxytol-enhanced LAVA images and confirm the hypermetabolic (yellow and red) tumor nodules. The marked contrast enhancement of the abdominal vessels enables clear localization of tumor nodules with regards to enhancing vessels.

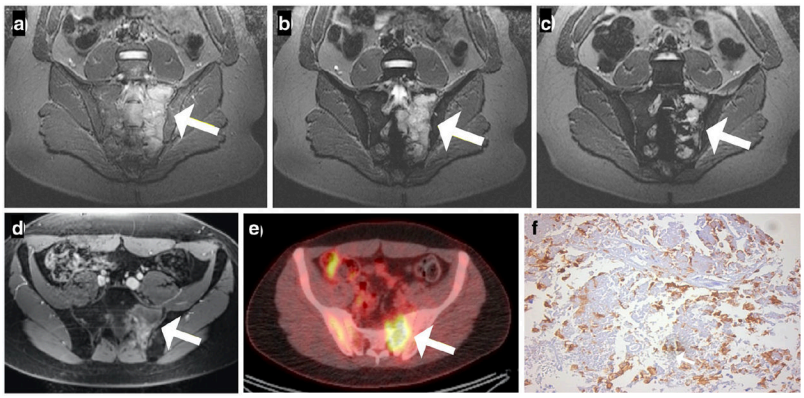

Figure 4: Comparison of tumor enhancement after intravenous administration of Gadolinium-chelate or ferumoxytol in a 15-year-old male with Ewing sarcoma of the left scapula:

(a) Axial T1-weighted fast spin echo (FSE) image demonstrates hypointense intra- and extraosseous soft tissue mass in the body of the left scapula. (b) Axial T1-weighted LAVA image after intravenous administration of Gadolinium-chelate demonstrates peripheral enhancement of the tumor tissue. (c) Axial T1-weighted LAVA image after intravenous administration of ferumoxytol demonstrates marked enhancement of the central tumor necrosis (arrow), which is hyperintense compared to muscle as an internal reference standard. (d) Simultaneously acquired axial ^{18}F-FDG PET image superimposed on T1-weighted ferumoxytol-enhanced LAVA image demonstrates the hypermetabolic (yellow) peripheral tumor tissue and central photopenic area of necrosis.

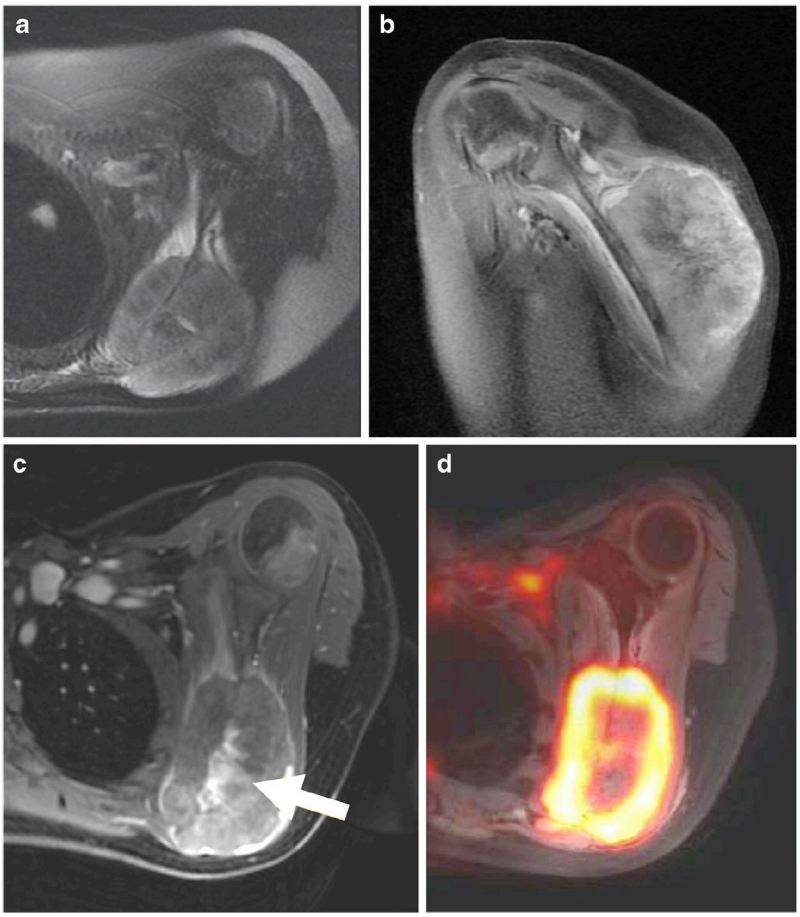

Figure 5: Ferumoxytol-enhanced MRI can estimate presence of tumor associated macrophages in a 24-year-old male patient with Ewing sarcoma in the sacrum.

(a) Oblique coronal T2-weighted FSE image before ferumoxytol injection shows hyperintense (bright) tumor signal (arrow) compared with skeletal muscle. (b) Oblique coronal T2-weighted FSE image at 30 minutes after intravenous ferumoxytol infusion demonstrates hypointense (dark) enhancement of the hematopoietic marrow and improved outline of the hyperintense tumors (arrow). (c) Oblique coronal T2-weighted FSE image at 24 hours after ferumoxytol infusion shows hypointense (dark) tumor signal enhancement (arrows). (d) Axial T1-weighted LAVA image after intravenous ferumoxytol injection demonstrates mild T1-enhancement of the tumor (arrow), less than muscle as an internal standard tissue. This limited T1-enhancement in conjunction with strong T2-enhancement suggests predominant intracellular localization of ferumoxytol nanoparticles in tumor associated macrophages. Note that the highly cellular bone marrow does not demonstrate any T1-effect. (e) Axial ^{18}F-fluorodeoxyglucose positron emission tomography / computed tomography (^{18}F-FDG PET/CT) demonstrates homogenous radiotracer uptake throughout the lesion (arrow). (f) Biopsy specimen of the tumor stained with CD163 mAb demonstrated multiple CD163 positive macrophages (brown staining) in the tumor tissue (20x magnification).

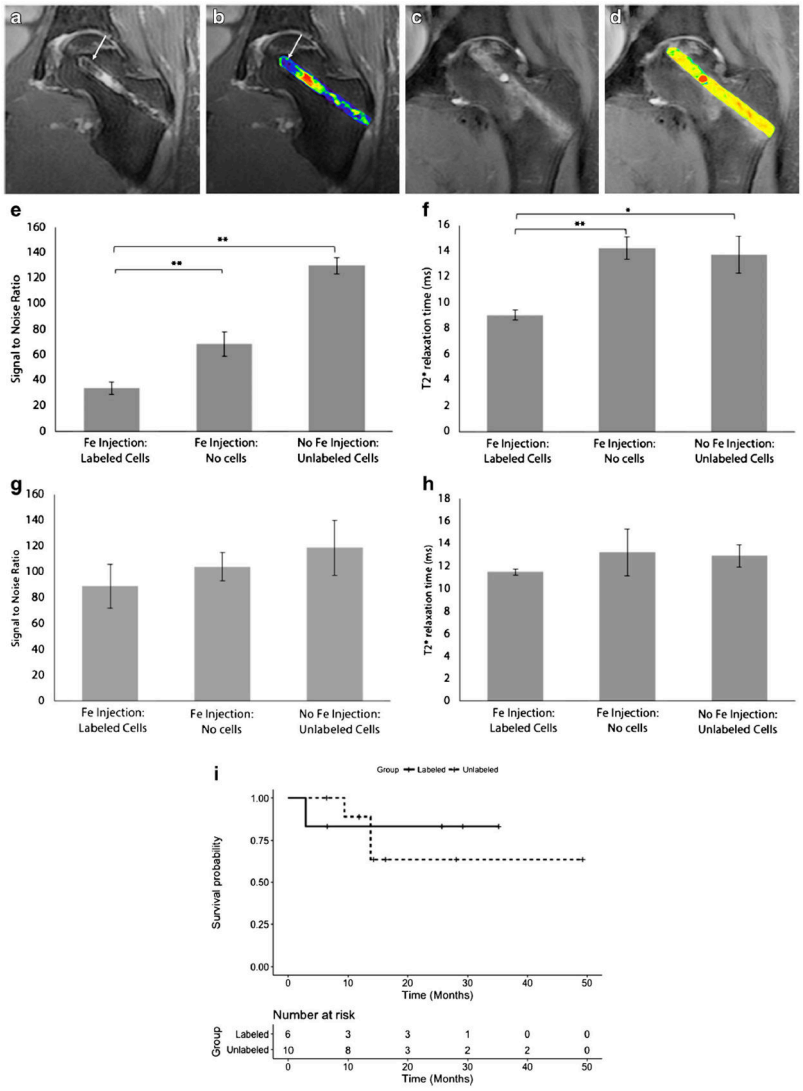

Figure 6:

Ferumoxytol-labeled cell transplants can be detected in the decompression track after core decompression. (a) Coronal T2-weighted MR image of the left femur of a patient who was treated with core decompression and injection of iron-labeled cells into the decompression track. Areas of hypointense (dark) signal (arrow) are noted in the decompression track, consistent with delivery of iron-labeled cells. (b) Superimposed color-coded signal intensities show areas of iron-labeled cells (arrow) as displayed by blue color. (c) Coronal T2-weighted MR of the left femur of a patient, who was treated with core decompression and injection of unlabeled cells into the decompression track. Unlabeled cells are noted by an intermediate signal in the decompression track. (d) Superimposed color-coded signal intensities show medium ranged signal intensities (green/yellow). Signal-to-noise ratios (SNR; e) and T2_ relaxation times (f) during the first week after surgery for areas that showed iron signal compared with areas where iron-labeled cells were not delivered and unlabeled controls show significantly lower SNR (P . 0.002, n . 18; P . 0.002, n . 10; respectively) and T2 relaxation times (P . 0.007, n . 9; P . 0.02, n . 6; respectively). SNR

(g) and T2_ relaxation times (h) at 4–7 weeks reveal no significant differences between the groups, suggesting interval iron metabolization. Data are mean ± standard error of the mean (SEM). P values were determined by mixed-effects model including a random effect term accounting for correlation among the measures within a same patient. (i) Time to progression of osteonecrosis between labeled and unlabeled cell transplants are not significantly different (P = 0.8, n = 16). P value was determined by log-rank test. (This figure has been reprinted with permission from Theruvath et al, Clin Ca Res 24(24): 6223-9; 2018).

Table 1:

Advantages and Limitations of Ferumoxytol-enhanced MRI

Ferumoxytol		
Advantages	**Possible Indication**	**Limitations**
- Iron supplement - Metabolization in the liver - Long lasting blood pool enhancement - Imaging vascular detail - Dwell time enables repeated scans - Uptake by normal liver - Uptake by Kupfer Cells - Uptake by normal spleen - Uptake by normal bone marrow - Leak across microvessels of malignant tumors - Uptake by tumor associated macrophages on delayed MRI - Leak into early necrosis - activates macrophages - can be used to track therapeutic cells	- Anemia - Patients with renal insufficiency - MR Angiography - Whole body MRI - Diagnosis of vascular malformations - Imaging congenital heart disease - Detection of malignant liver lesions - Differentiation of HCC and FNH - Detection of splenic tumors - Detection of bone marrow tumors - Differentiation between benign and malignant tumors - Imaging response to macrophage modulating immunotherapy - Detection of early necrosis - inhibits early tumor growth - in vivo tracking of therapeutic cells	- Contraindicated in patients with iron overload - can rarely cause severe allergic reactions - can cause complement activation related pseudoallergy (CARPA) - No bolus injection - Slow infusion over 15 minutes - Slow metabolization - repeated imaging after 6-8 weeks - Less T1-enhancement of most solid tumors compared to Gd-enhancement - can enhance inflammatory reactions - can cause diagnostic confusion due to leak into early necrosis